by hillslopes that are much less steep.

In each of these examples, baselevel lowering has led to destabilization of the bounding hillslopes, resulting in steep toes that may coalesce along the channel to form inner gorges. Our experiments show that an inner gorge may well represent part of the natural development of hillslopes, rather than indicate tectonic or climatic rejuvenation. Because slope-clearing events are rare, instantaneous hillslope profiles will most likely show the steepened toes formed by smaller landslides. The detailed hillslope morphology, as well as the gross relief (*11*), may thus be a quantitative measure of the landscape-scale rock strength, at least in cases where this strength is controlled by discontinuities.

Hillslope profiles in the physical model are independent of the rate of boundary drop; no time scale is involved. We expect different system behavior if dynamic forces such as earthquakes are introduced, or if the strength of the rock mass is time dependent. If the rate of generation of low-strength fractures and joints is much higher than the rate of stripping, there will always be sufficient material of relatively low cohesion to yield deep-seated landslides, and we would expect hillslopes to evolve as in our experiments.

REFERENCES AND NOTES

1. M. L. Stout, *Geol. Soc. Am. Abstr. Programs* **16**, 257 (1984); P. C. Augustinus, *Earth Surf. Process. Land*. **17**, 39 (1992); J. M. Harbor, *Geol. Soc. Am. Bull.* **104**, 1364 (1992); S. W. Nelson, *U.S. Geol. Surv. Bull*. **2107**, 43 (1993); N. Hovius, C. P. Stark, P. A. Allen, *Geology*, in press.
2. H. M. Kelsey, *Geol. Soc. Am. Bull*. **91**, Part II, 1119 (1980).
3. _____, *Catena* **15**, 433 (1988).
4. R. S. Anderson, *J. Geophys. Res*. **99**, 20161 (1994).
5. D. W. Burbank *et al*., *Nature* **379**, 505 (1996).
6. H. Kooi and C. Beaumont, *J. Geophys. Res.* **101**, 3361 (1996).
7. A. D. Howard, *Water Resour. Res*. **30**, 2261 (1994); G. E. Tucker and R. L. Slingerland, *J. Geophys. Res*. **99**, 12229 (1994).
8. K. Terzaghi, *Geotechnique* **12**, 251 (1962); M. J. Selby, *Z. Geomorphol.* **24**, 31 (1980).
9. M. J. Kirkby, in *Slope Stability: Geotechnical Engineering and Geomorphology*, M. G. Anderson and K. S. Richards, Eds. (Wiley, Chichester, UK, 1987), pp. 359–379.
10. D. J. Miller, thesis, University of Washington, Seattle (1993).
11. K. M. Schmidt and D. R. Montgomery, *Science* **270**, 617 (1995).
12. M. G. Wolman and J. P. Miller, *J. Geol*. **68**, 54 (1960).
13. A. B. Gibbons, J. D. Megeath, K. L. Pierce, *Geology* **12**, 327 (1984).
14. M. J. Selby, *Hillslope Materials and Processes* (Oxford Univ. Press, Oxford, 1993); J. R. Arrowsmith, D. D. Pollard, D. D. Rhodes, *J. Geophys. Res*. **101**, 6255 (1996).
15. The model consisted of two parallel, clear acrylic plates, each 51 cm by 38 cm by 0.6 cm thick. The 2.5-cm space separating the plates was filled with a granular material. Baselevel for the hillslope was determined by a sliding acrylic strip that formed one wall of the model (the active boundary), which was lowered at 0.5-cm intervals. Because all material reaching the toe of the hillslope was removed, no buttressing of the hillslope was allowed. The mass of the removed material was measured on a digital balance with a precision of ±0.1 g.
16. See reviews in S. K. Grumbacher, K. M. McEwen, D. A. Halverson, D. T. Jacobs, J. Lindner, *Am. J. Phys*. **61**, 329 (1993); J. M. Carlson and G. H. Swindle, Proc. *Natl. Acad. Sci. U.S.A.* **92**, 6712 (1995).
17. This lowering could result from fluvial or glacial incision, by sea- or lake-level fall, or by dip-slip motion on a fault.
18. For example, V. Frette *et al*., *Nature* **379**, 49 (1996).
19. We also evaluated the effect of structural dip on slide behavior [K. Terzaghi in (*8*); S. R. Hencher, in *Slope Stability: Geotechnical Engineering and Geomorphology*, M. G. Anderson and K. S. Richards, Eds. (Wiley, Chichester, UK, 1987), pp. 145–186] by creating horizontal stratigraphy and then tilting the entire model, either toward or away from the active boundary. This created either a dip-slope or antidip-slope, respectively.
20. The length of the hillslope imposed an upper bound on the size of a slide. By reporting only those results from the steady phase, we ensured that observed temporal variations in slide size were not due to changes in hillslope length.
21. J. Rosendahl, M. Vekic, J. Kelley, *Phys. Rev. E* **47**, 1401 (1993).
22. This agreed with observations of real hillslopes [W. F. Megahan, N. F. Day, T. M. Bliss, in *Forest Soils and Land Use; Proceedings of the Fifth North American Forest Soils Conference*, C. T. Youngberg, Ed. (Colorado State Univ., Ft. Collins, CO, 1978), pp. 116–139; (*2*)].
23. K. Shimazaki and T. Nakata, *Geophys. Res. Lett*. **7**, 279 (1980).
24. In contrast, time-predictable behavior would imply the existence of a threshold strength or steep toe height that must be exceeded before failure occurs. We saw no evidence for such a threshold.
25. Slides in the dip-slope experiments were smaller and more frequent than in the horizontal experiments for both red and white beans. We attributed this to the higher probability of favorably oriented failure planes in the dip-slope experiments [for example, Terzaghi (*8*)], which aided sliding and prevented large accumulations of material on the hillslope. By contrast, slides were much less frequent in the antidip-slope experiments because of the paucity of potential failure planes. Antidip-slope slides were also smaller than in the horizontal experiments, demonstrating the difficulty of removing material without favorably oriented failure planes.
26. S. M. Cashman, H. M. Kelsey, D. R. Harden, *U.S. Geol. Surv. Prof. Pap. 1454* (1995), pp. B1–B12.
27. B. G. McAdoo, D. L. Orange, E. Screaton, R. Kayen, H. Lee, *Am. Assoc. Pet. Geol. Bull.* **80**, 605 (1996).
28. L. F. Pratson and B. J. Coakley, *Geol. Soc. Am. Bull*. **108**, 225 (1996).

29. We thank D. Stakes of MBARI for access to her workstation and data visualization software; S. Anderson, G. Dick, K. Howard, and J. Repka for helpful discussions; H. Kelsey for observations and advice; and two anonymous reviewers for their comments. Supported by NASA Earth Systems Science graduate fellowship NGT-51220 to A.L.D. and by a grant from the NASA Surface Change Program. SeaBeam data collection and ALVIN dives were supported by Office of Naval Research grant N00014-9301-202.

22 August 1996; accepted 4 November 1996

An Explanation for Earth's Long-Term Rotational Stability

Mark A. Richards, Yannick Ricard, Carolina Lithgow-Bertelloni, Giorgio Spada, Roberto Sabadini

Paleomagnetic data show less than ~1000 kilometers of motion between the paleomagnetic and hotspot reference frames—that is, true polar wander—during the past 100 million years, which implies that Earth's rotation axis has been very stable. This long-term rotational stability can be explained by the slow rate of change in the large-scale pattern of plate tectonic motions during Cenozoic and late Mesozoic time, provided that subducted lithosphere is a major component of the mantle density heterogeneity generated by convection. Therefore, it is unnecessary to invoke other mechanisms, such as sluggish readjustment of the rotational bulge, to explain the observed low rate of true polar wander.

Movement of the Earth with respect to its axis of rotation on long time scales (10^3 to 10^9 years) is called polar wander, as distinguished from shorter term periodic or transient fluctuations, which are called wobble (*1*). Assuming that the average paleomagnetic axis corresponds to the paleorotation axis, paleomagnetic data can be used to measure the path of polar wander over continents or plates, which results mainly from plate tectonic motions. Paleomagnetic data can also be used to measure polar wander with respect to volcanic hotspots, such as Hawaii or Iceland, which appear to remain relatively fixed with respect to the more rapid global plate motions (*2*). This true polar wander (TPW) is generally taken as evidence that the mass redistribution resulting from mantle convection causes relative motion between Earth's principal inertia axis and the deep mantle source region for hotspots (*3*). Therefore, the paleomagnetic record of TPW provides a temporal constraint on

M. A. Richards, Department of Geology and Geophysics, University of California, Berkeley, CA 94720, USA.
Y. Ricard, Departement de Geologie, Ecole Normale Superieure, Lyon, France.
C. Lithgow-Bertelloni, Department of Terrestrial Magnetism, Carnegie Institution of Washington, Washington, DC 20015–1305, USA.
G. Spada, Dipartimento di Fisica, Settore Geofisica, Universita di Bologna, Bologna, Italy.
R. Sabadini, Dipartimento di Scienze della Terra, Sezione Geofisica, Universita di Milano, Milano, Italy.

models of mantle convection and plate tectonics.

Measurement of TPW is indirect and somewhat controversial. One method is to form the difference between the apparent polar wander paths of a continent in the hotspot and paleomagnetic reference frames. For example, calculated TPW paths (*4*–*6*) show that the paleomagnetic pole has moved with respect to hotspots (Fig. 1A) by only about 10° of latitude since ~100 million years ago (Ma). Error estimates are generally on the order of ~5° or more, and the various analyses give somewhat different TPW paths; however, there appears to be a resolvable motion of the rotation axis with respect to hotspots of about 5° to 10° toward Greenland (in modern geographic coordinates) since early Tertiary time (~50 to 60 Ma), preceded by motion of about 10° to 15° away from Greenland since mid-Cretaceous time (~100 Ma) (*7*). Thus, the rate of TPW in recent Earth history has been only about 0.1° to 0.2° per million years. Rates of TPW before about 90 to 100 Ma may have been several times more rapid, but paleomagnetic data from hotspots this age and older are fewer in number and are subject to large errors (*1*).

Earth's inertia tensor is most likely controlled by internal mass rearrangements attributable to mantle convection, and it is surprising that there has been so little TPW since late Mesozoic time (*8*, *9*). Simple isoviscous mantle (upper and lower mantle viscosity being equal) convection models predict polar wander rates on the order of 1° to 10° per million years when the models are scaled to Earth-like parameters for viscosity, heat production, and surface plate velocities (*10*). Two plausible explanations for the much slower observed rate of TPW have been suggested: (i) Earth's internal density structure changes on a time scale significantly longer than that associated with surface plate motions (*1*, *11*), and (ii) the lower mantle is of sufficiently high viscosity to inhibit relaxation of Earth's rotational bulge, thus filtering out, in time, more rapid fluctuations in the planet's inertia tensor (*8*, *12*–*14*). However, such long relaxation times imply that the average mantle viscosity is at least an order of magnitude larger than that inferred from studies of postglacial rebound and that the ratio of lower to upper mantle viscosity is much larger than that allowed by geoid models (*15*). Here, we show that the slow rate of change of Earth's internal density structure may explain the slow observed rate of TPW by modeling the recent evolution of mantle density heterogeneity and its effect on rotational dynamics.

Problems of rotational dynamics can be understood with the use of the Liouville equation (*16*), which describes the conservation of angular momentum for a rotating body in the absence of external torques in a body-fixed (noninertial) reference frame

$$\frac{d}{dt}(\mathbf{J}\cdot\boldsymbol{\omega}) + \boldsymbol{\omega}\times\mathbf{J}\cdot\boldsymbol{\omega} = 0 \qquad (1)$$

where $\boldsymbol{\omega}$ is the angular velocity vector, the derivative is with respect to time t, and the time-dependent second-order symmetric inertia tensor $\mathbf{J}$ is given by

$$J_{ij}(t) = I\delta_{ij} + \frac{k^{T}(t)R^{5}}{3G} * [\omega_i(t)\omega_j(t) - \frac{1}{3}\omega^2(t)\delta_{ij}] + [\delta(t) + k^{L}(t)] * C_{ij}(t) \qquad (2)$$

where $\delta(t)$ is the Dirac function, G the gravitational constant, δ_{ij} the Kronecker delta function, and * indicates a convolution in time (*13*). The first term of Eq. 2 is the main inertia I of a spherically symmetric Earth, which is about $0.33MR^2$, where M and R are Earth's mass and mean radius, respectively. The second term describes the effect of centrifugal deformation (the rotational "bulge"), which is on the order of 10^{-3} MR^2 and involves a tidal Love number k^{T}, whose limit for the time scale of interest here is referred to as the tidal fluid Love number (*16*). This Love number accounts for the effect of self-gravitation on Earth's rotational figure. The centrifugal term therefore limits the TPW velocity because the rotational axis can change only as fast as Earth's rotational bulge relaxes by means of viscous mantle flow (*8*, *13*). The third term in Eq. 2 represents changes in inertia due to internal mass rearrangement $\mathbf{C}$ and is on the order of 10^{-5} MR^2 for mantle convection processes. This term also involves viscous deformation of the Earth due to internal mass anomalies through the spherical harmonic degree 2 loading Love number k^{L}, which accounts for the surface and core-mantle boundary topography induced by loading (*17*). The nonlinear Euler equations 1 can be solved numerically (*13*) given an excitation-function time history $\mathbf{C}(t)$ and a viscosity model of Earth's mantle, for calculating k^{L} and k^{T} (*18*).

True polar wander can be caused by changes in the inertia tensor due to internal mass redistribution, which can be expressed in terms of $\mathbf{C}(t)$. These changes can arise from a variety of mechanisms, such as mantle convection, plate motions, or glacioisostatic adjustment. Although TPW on the 1000- to 100,000-year time scale can be strongly affected by glacial isostasy, these fluctuations probably average out on longer time scales (*19*); thus, longer term TPW almost certainly results from mantle convection.

The largest changes in mantle mass heterogeneity attributable to convection are probably caused by subduction, which injects cold slabs of the lithospheric thermal boundary layer into the mantle where plates converge. Subduction zones can be mapped reasonably well from global plate reconstructions for Cenozoic and late Mesozoic time (*20*, *21*). We

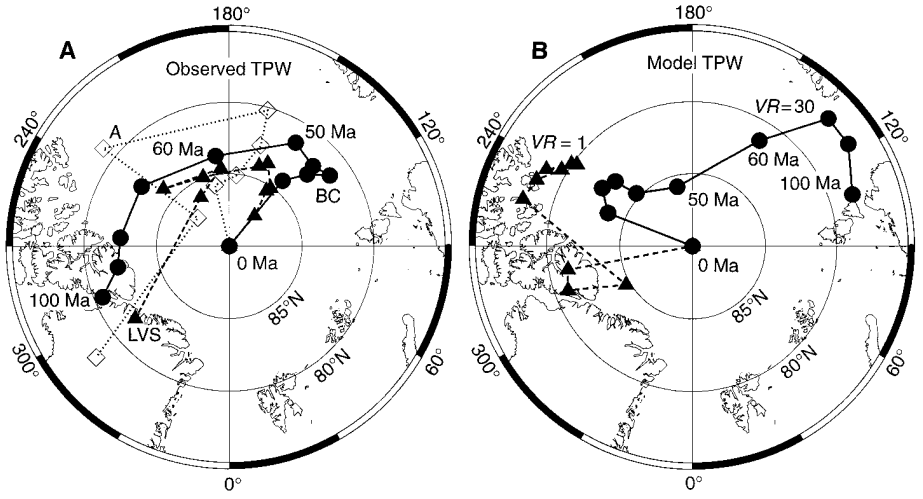

Fig. 1. (**A**) Motion of Earth's rotation axis with respect to hotspots, as deduced from the paleomagnetic data of Besse and Courtillot (*6*) (BC: solid circles), Livermore, Vine, and Smith (*4*) (LVS: solid triangles), and Andrews (*5*) (A: open diamonds). Symbols are given at 10-Ma time intervals, with the 0, 50, 60, and 100 Ma times for the BC curve labeled. Error ellipses are not shown because they would render the plot unreadable, but they were typically about 5° to 10° of latitude in diameter (*4*–*6*). For reference, a 10° error ellipse would completely fill the area within the 85°N circle, so the details of the various curves are not well resolved. (**B**) Motion of Earth's rotation axis with respect to hotspots, computed for the isoviscous (VR = 1: solid triangles) and layered viscosity (VR = 30: solid circles) models. Symbols are given at 10-Ma intervals, with the 0, 50, 60, and 100 Ma times for the VR = 30 case labeled. These computations are compensated (*26*), so that the present-day model rotation axis corresponds to the North Pole.

used paleosubduction zones to infer mantle heterogeneity changes, following a modeling strategy used to account for the shape of Earth's gravity field (geoid), global plate motions, and much of the observed seismic heterogeneity structure of the mantle (*15, 22, 23*). Although other mantle heterogeneity sources are present—for example, mantle plumes associated with volcanic hotspots—the use of maps of ancient subduction zones to model polar wander represents a minimum in terms of temporal internal mass fluctuations due to mantle convection.

Our time-dependent model of mantle mass heterogeneities attributable to subduction (*15, 20, 22*) includes (i) locating subduction zones in the hotspot reference frame since 200 Ma using published plate reconstructions, (ii) computing the mass anomalies sinking along ancient trenches according to local subduction rates and a model of the thermal structure of oceanic lithosphere (*15, 22*), and (iii) allowing these subducted mass anomalies to sink through the mantle at their initial rate of convergence (whole mantle convection is assumed). For cases in which the viscosity of the lower mantle was higher than that of the upper mantle, we slowed the sinking of the slabs as they entered the lower mantle by an empirical factor, which was chosen to give good agreement with independent geophysical observations. In previous work (*15, 23*), we showed that slowing the sinking of slabs by a factor of about 4 in the lower mantle fits seismic heterogeneity and the nonhydrostatic geoid and yields a reasonable dynamical model of global Cenozoic plate motions. This factor of 4 is also consistent with constraints on mantle viscosity structure, which suggest an increase by about a factor of 30 to 100 in mantle viscosity with depth (*24*). [Slab sinking velocities are expected to scale roughly with the log of the viscosity contrast (*25*).]

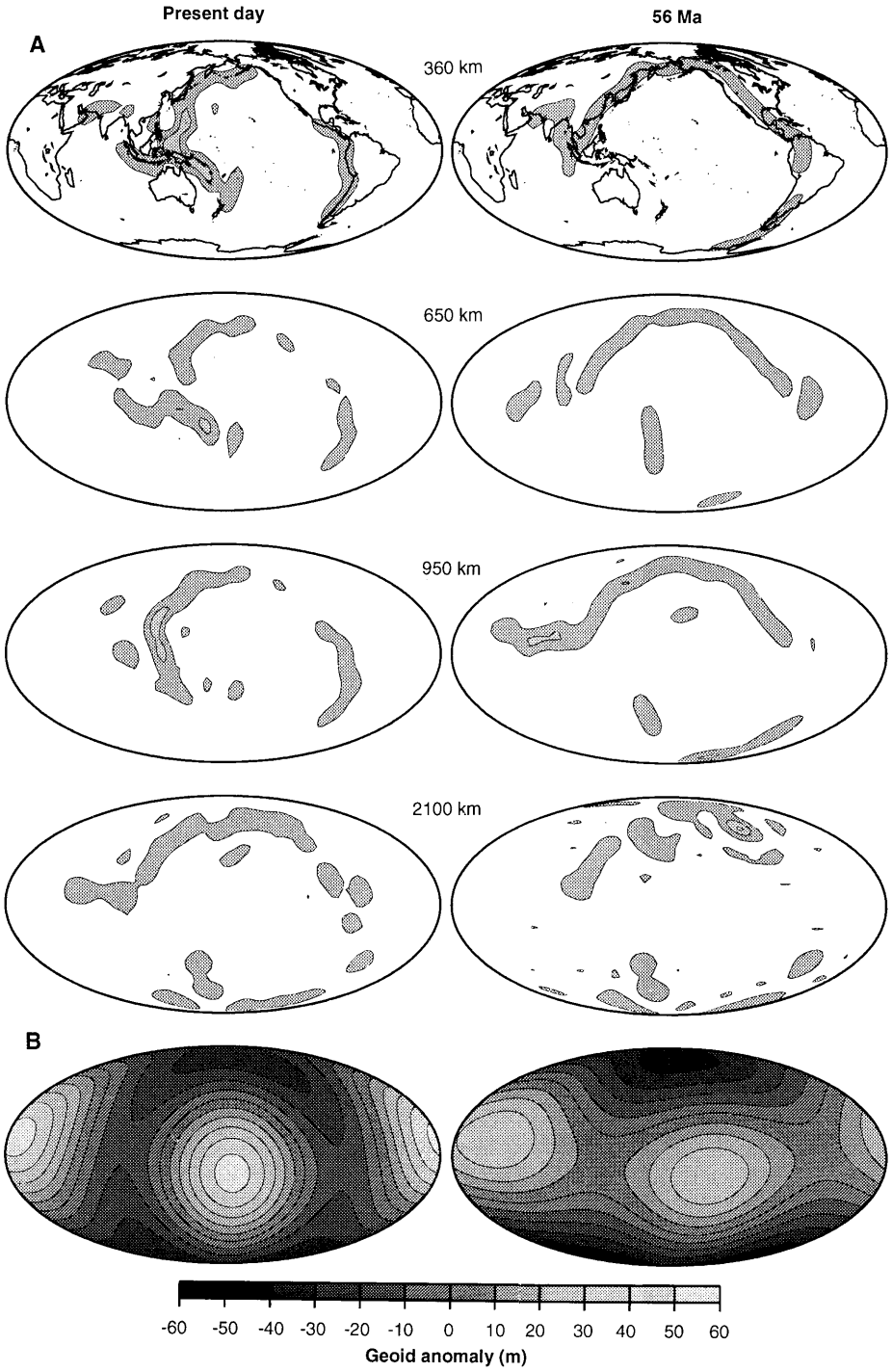

Fig. 2. (**A**) Time snapshots of the subduction heterogeneity model (degree $l = 20$) (*15, 20, 22*) for the present day and 56 Ma. The gray areas indicate the presence of cold slabs at various depths in the mantle in the hotspot reference frame. (**B**) The degree 2 geoid at 0 and 56 Ma, illustrating that the degree 2 inertia tensor has probably changed little since the early Tertiary.

Our model leads to a time-dependent mantle heterogeneity field, which for our purposes becomes the excitation function **C** and drives polar wander in the hotspot reference frame. Snapshots of this model at various mantle depths for the present day and 56 Ma (Fig. 2A) mimic the downward projection of ancient and modern subduction zones, with the deeper slabs generally being older. Although there are fine-scale fluctuations, the large-scale, largely circum-Pacific pattern of subduction has not changed much since the beginning of Cenozoic time. This fact is emphasized in a comparison of the harmonic degree 2 geoids predicted by the slab model at the same times (Fig. 2B). The degree 2 geoid—involving an integral of mass heterogeneities over the depth of the mantle—changes very little in shape during this time interval, which means that the inertia excitation function **C** also changes little. The inertia tensor is linearly related to the degree 2 geoid coefficients (*16*). This result suggests, before any rotational dynamics calculations, that subduction itself may cause little Cenozoic TPW.

Full dynamical calculations based on the solution of Eqs. 1 and 2 confirm this prediction. In the simplest, isoviscous model (Fig. 3) (upper mantle viscosity = 10^{21} Pa·s, lower/upper mantle viscosity ratio $VR = 1$), slabs sink through the entire mantle at a uniform rate. For viscosity ratios of $VR = 30$ and 100, we slowed the slabs by a factor of 4 as they sank into the lower mantle. The layered viscosity models give smoother TPW curves than does the isoviscous model. This smoothness results mainly from the effect of slowing

the slabs' sinking velocities in the lower mantle, not from sluggish relaxation of the rotational bulge in response to changes in inertia. The bulge effect is present in our calculations, but the changes in **C** due to subduction were so slow during the last 60 million years that the relaxation of the bulge was not the limiting factor; it is mainly the slow variation in **C** that controls the rates of polar wander. All three models yield similar amounts of long-term polar wander, especially over the past 60 million years, when rates were always less than 1° per million years. For the $VR = 30$ model, the rates were <0.5° per million years since the beginning of the Tertiary, with only about 10° total latitudinal drift of the rotation axis since 50 Ma, or an average of about 0.2° per million years, a rate that falls within the observational constraints on TPW (Fig. 1A). The $VR = 30$ model also gives a good fit to the present-day geoid (*15*).

Comparison (Fig. 1B) of the polar wander paths predicted by isoviscous ($VR = 1$) and layered viscosity ($VR = 30$) models in the same reference frame (*26*) as that for the observed paths (Fig. 1A) shows a strong sensitivity of the TPW path to variations in viscosity structure. Although the details of the various observed curves also vary greatly, the $VR = 30$ model does yield a reasonable overall amplitude for TPW since 100 Ma, and the predicted TPW since the early Tertiary (50 to 60 Ma) is about 5° to 10° toward Greenland, roughly in accord with observation. The latter result is also consistent with Jurdy's (*27*) empirical analysis of polar wander resulting from changes in Cenozoic subduction. The model paths for before Tertiary time are not very meaningful because subduction history becomes less well constrained in the time frame of 100 to 200 Ma. Nevertheless, the low observed rate of TPW is explained by relatively slow changes in the global pattern of subduction zones.

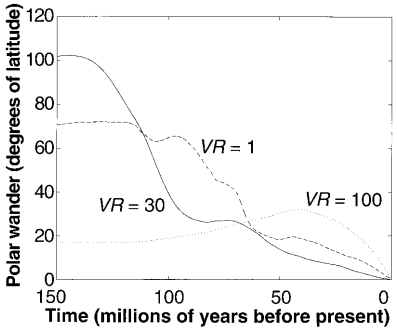

Fig. 3. Distance in degrees (latitude) between the position of the rotation axis at time zero (present) and the position at times in the past for the three different mantle viscosity models. These curves are computed from solutions to the full, nonlinear Euler equations 1 given in (*13*).

REFERENCES AND NOTES

1. R. G. Gordon, *Annu. Rev. Earth Planet. Sci.* **15**, 567 (1987).
2. W. J. Morgan, in *The Sea*, C. Emiliani, Ed. (Wiley, New York, 1981), vol. 7, pp. 443–487.
3. D. M. Jurdy, *Tectonophysics* **74**, 1 (1981).
4. R. A. Livermore, F. J. Vine, A. G. Smith, *Geophys. J. R. Astron. Soc.* **79**, 939 (1984).
5. J. Andrews, *J. Geophys. Res.* **90**, 7737 (1985).
6. J. Besse and V. Courtillot, *ibid.* **96**, 4029 (1991).
7. This long-term TPW is in the same direction as, although much smaller in amplitude than, the present-day polar wander, which is attributed to postglacial rebound. See, for example, S. R. Dickman, *Geophys. J. R. Astron. Soc.* **51**, 229 (1977); (*19*).
8. T. Gold, *Nature* **175**, 526 (1955).
9. P. Goldreich and A. Toomre, *J. Geophys. Res.* **74**, 2555 (1969).
10. P. J. Tackley, thesis, California Institute of Technology (1994); M. A. Richards, Y. Ricard, H.-P. Bunge, *Eos* **75**, 67 (1994); in preparation.
11. C. G. Chase, *Annu. Rev. Earth Planet. Sci.* **13**, 97 (1985).
12. G. Spada, Y. Ricard, R. Sabadini, *Nature* **360**, 452 (1992).
13. Y. Ricard, G. Spada, R. Sabadini, *Geophys. J. Int.* **113**, 284 (1993).
14. R. Sabadini, D. A. Yuen, E. Boschi, *J. Geophys. Res.* **89**, 7609 (1984); R. Sabadini and D. A. Yuen, *Nature* **339**, 373 (1989).
15. Y. Ricard, M. A. Richards, C. Lithgow-Bertelloni, Y. LeStunff, *J. Geophys. Res.* **98**, 21895 (1993).
16. W. Munk and G. J. F. MacDonald, *The Rotation of the Earth: A Geophysical Discussion* (Cambridge Univ. Press, London, 1960).
17. M. A. Richards and B. H. Hager, *J. Geophys. Res.* **89**, 5987 (1984); Y. Ricard, L. Fleitout, C. Froidevaux, *Ann. Geophys.* **2**, 267 (1984).
18. G. Spada, thesis, University of Bologna (1992).
19. R. Sabadini and W. R. Peltier, *Geophys. J. R. Astron. Soc.* **66**, 553 (1981).
20. M. A. Richards and D. C. Engebretson, *Nature* **355**, 437 (1992).
21. D. C. Engebretson, K. P. Kelly, H. J. Cashman, M. A. Richards, *GSA Today* **2**, 93 (1992).
22. C. Lithgow-Bertelloni and M. A. Richards, *Rev. Geophys.*, in press.
23. ———, *Geophys. Res. Lett.* **22**, 1317 (1995).
24. B. H. Hager and M. A. Richards, *Philos. Trans. R. Soc. London Ser. A* **328**, 309 (1989); S. D. King and T. G. Masters, *Geophys. Res. Lett.* **19**, 1551 (1992); J. X. Mitrovica, *J. Geophys. Res.* **101**, 555 (1996).
25. M. Gurnis, thesis, Australian National Univ. (1986); M. A. Richards, in *Glacial Isostasy, Sea Level and Mantle Rheology*, R. Sabadini *et al.*, Eds. (Kluwer Academic, Hingham, MA, 1991), pp. 571–588.
26. The polar wander paths in Fig. 1B are calculated somewhat differently than the simpler latitudinal variation curves in Fig. 3. In Fig. 1B, we have compensated for the fact that the subduction heterogeneity model does not yield the correct present-day degree 2 geoid (for example, the C_{21} and S_{21} harmonic coefficients are nonzero). This mismatch results from model error of an undetermined nature (*15*). The compensation is achieved by subtracting the mismatched off-diagonal terms in the present-day inertia tensor from the calculations at all times, so that the present-day model rotation pole position corresponds exactly to Earth's North Pole; otherwise, the model and observed curves would not be comparable in any meaningful way because the model curves would begin at some latitude different from the North Pole. This solution is not entirely satisfactory, but it provides a way to compare the overall amplitudes of the TPW curves. Comparison between the detailed shapes of the observed and model TPW paths are probably not very meaningful because of the uncertainties in observations and the necessary compensation of the model curves.
27. D. M. Jurdy, *J. Geophys. Res.* **88**, 6395 (1983).

28. M.A.R. was supported by NSF grants EAR-9117538 and EAR-9629376 and is grateful to C. Froidevaux of the Ecole Normale Superieure, Paris, for support as a visiting scholar. R. Gordon and D. Jurdy provided helpful reviews of the original manuscript.

12 August 1996; accepted 22 November 1996

Depletion of the Outer Asteroid Belt

Jer-Chyi Liou* and Renu Malhotra

During the early history of the solar system, it is likely that the outer planets changed their distance from the sun, and hence, their influence on the asteroid belt evolved with time. The gravitational influence of Jupiter and Saturn on the orbital evolution of asteroids in the outer asteroid belt was calculated. The results show that the sweeping of mean motion resonances associated with planetary migration efficiently destabilizes orbits in the outer asteroid belt on a time scale of 10 million years. This mechanism provides an explanation for the observed depletion of asteroids in that region.

Asteroids are small, rocky bodies less than 1000 km in diameter that lie between the orbits of Mars and Jupiter in the region traditionally called the asteroid belt. The outer asteroid belt, from 3 to 5 astronomical units (AU) from the sun, is nonuniform and depleted of asteroids. The orbital eccentricities and inclinations, as functions of semi-major axes, of 7100 numbered asteroids (*1*) (Fig. 1) show four major features: (i) a lack of asteroids in the 1:2 interior mean motion resonance (MMR) (*2*) with Jupiter centered at 3.28 AU, (ii) a lack of asteroids between 3.5 and 3.9 AU, (iii) a concentration of asteroids in the 2:3 interior MMR with Jupiter centered at 3.97 AU, and (iv) a lack of asteroids beyond the 2:3 interior MMR.

The "gravitational hypothesis" (*3*) postulates that the gravitational forces of the planets are responsible for shaping the asteroid belt. This hypothesis has explained

J.-C. Liou, SN3, NASA Johnson Space Center, Houston, TX 77058, USA.
R. Malhotra, Lunar and Planetary Institute, Houston, TX 77058, USA.

*To whom correspondence should be addressed. E-mail: liou@sn3.jsc.nasa.gov